Ice nucleation on a corrugated surface

Chenfang Lin[†], Gefen Corem[‡], Oded Godsi[‡], Gil Alexandrowicz[‡◊], George R. Darling[†] and Andrew Hodgson[†*]

[†]*Surface Science Research Centre and Department of Chemistry, University of Liverpool, Liverpool L69 3BX, UK*

[‡] *Shulich Faculty of Chemistry, Technion, Haifa 32000, Israel*

[◊]*Department of Chemistry, Swansea University, Singleton Park, Swansea SA2 8PP, UK.*

Communicating author: *ahodgson@liverpool.ac.uk

Supporting Material

1. Water adsorption and characterization of the (3 0, -1 1) phase at 1 ML coverage.
2. Structure calculations and adsorption energies for the hexagonal, 1 ML water network.
3. Additional structures calculated for 2 and 3 ML of water.
4. Entropic contributions to the free energy of 2D versus 3D structures.

1. Water adsorption and characterization of the (3 0, -1 1) phase at 1 ML coverage.

TPD profiles recorded as a function of the coverage (Fig. S1a) show formation of a first layer desorption peak that is approximately zero order and saturates in intensity with a peak maximum near 173 K. Increasing the water dose forms a multilayer, characterized by the appearance of a desorption peak above 150 K. The multilayer peak is zero order, having a common leading edge that persists as thick films are grown. No evidence was found of any change in multilayer desorption rate with coverage that could be associated with crystallization of the ice film, consistent with LEED showing the ice multilayer is ordered at all temperatures ≥ 120 K. The barrier to desorption was obtained from a leading edge analysis and is plotted against coverage in Fig. S1b, along with the surface symmetry obtained from LEED.

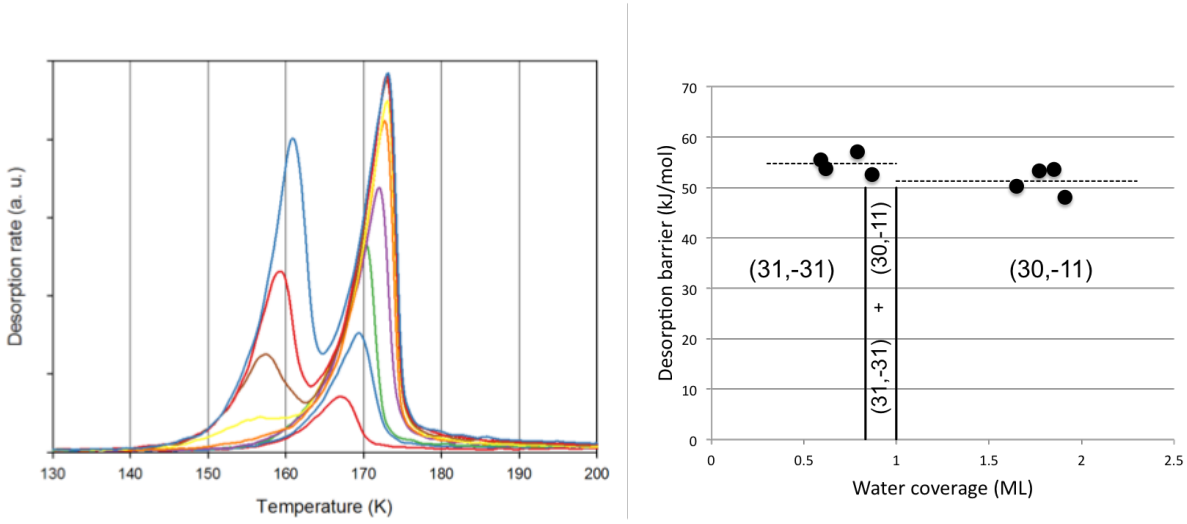

Figure S1 a) TPD of water from Cu(511) as a function of the water coverage showing the monolayer peak saturating near 173 K and the multilayer peak forming above 150 K as the water coverage exceeds 1 ML coverage (heating rate 1 Ks^{-1}, 0.20, 0.41, 0.62, 0.88, 1.02, 1.13, 1.34, 1.56 and 1.85 ML water). b) Water phase diagram indicating the LEED pattern observed as a function of coverage and the activation energy for water desorption, measured from a leading edge analysis of the TPD curves.

Ordering of the water layer was mapped as a function of coverage using a low current LEED system (OCI), equipped with a dual multichannel plate electron multiplier stage. The electron beam spot was deliberately defocused to reduce the current density. LEED patterns were recorded at currents down to ca. 1 nA, providing diffraction patterns free from electron damage. Extended exposure to the electron beam, or increased currents, caused electron damage and degraded the LEED patterns. The absolute water coverage was calibrated based on the LEED pattern and the structure of the 0.833 ML (3 1, -3 1) phase, established by STM and DFT[1]. This calibration was consistent with the absolute flux of the molecular beam determined in previous measurements on ordered water films[2-4]. Diffraction beams corresponding to the (3 1, -3 1) water islands appear above ca. 0.3 ML and reach a maximum as the structure completes at 0.833 ML water. The first layer water TPD peak continues to grow larger, with TPD showing ~25% more water is incorporated in the film to give a coverage of 1.0 ML before the multilayer peak finally appears. The (3 1, -3 1) diffraction beams (Fig. 2a) slowly disappear above 0.83 ML as the film incorporates more water, the LEED pattern changing to a (3 0, -1 1) structure (Fig. 2c) that persists from 1 ML to higher coverage. Helium reflectivity was recorded as a function of surface coverage and shows the same change from a (3 1, -3 1) diffraction pattern below saturation coverage[1] to the (3 0, -1 1) HAS pattern shown in Fig 2b as the first layer saturates with water.

A large scale STM image of the completed (3 0, -1 1) 1 ML structure is shown in Fig. S2a and is dominated by ordered features corresponding to H-up water that is aligned in rows long the $[0\bar{1}1]$ step direction. The Fourier transform of the STM image is shown in Figure S2b and has intense peaks at the first order positions corresponding to the Cu step spacing and weak peaks corresponding to other (3 0, -1 1) diffraction positions. Frames S2c,d show the Fourier transform of regions dominated by the hexagonal and rectangular arrangements respectively. The hexagonal region (c) shows 6 first order and 4 second order peaks, which are also present weakly in (b), while the rectangular region shows the first order peaks across the steps and half order peaks along the steps, with higher order peaks being weak. The first order peaks across the step direction are common to both structures and remain intense in the large area image, but the half order features of the rectangular superstructure disappear with only weak peaks persisting at the (3 0, -1 1) positions. Like STM, HAS is sensitive to the top layer and shows weak diffraction features at the (3 0, -1 1) positions (Fig. 2). LEED shows an intense (3 0, -1 1) diffraction pattern, as it is sensitive to the O position and Cu relaxation, rather than the H location.

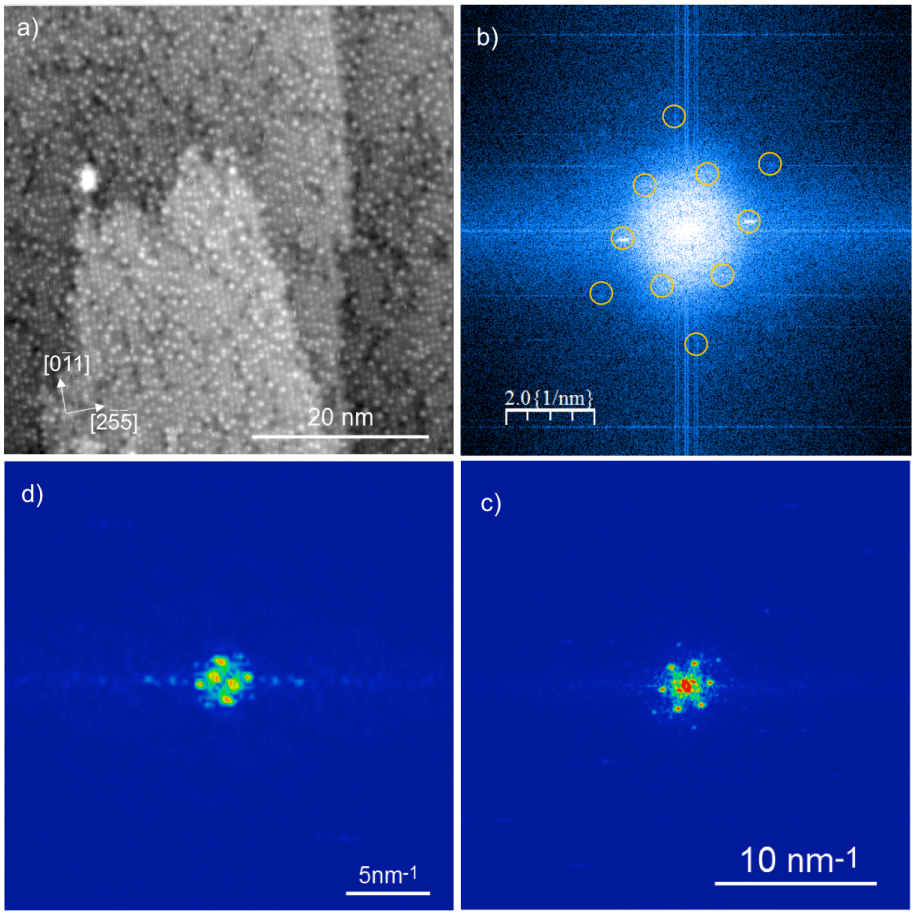

Figure S2. a) large scale STM image of the (3 0, -1 1) structure shown in Fig. 2d and b) the Fourier transform of this image. c) shows the Fourier transform of a smaller region dominated by the hexagonal ordering of the H-up water (see Fig. 3) and d) for a rectangular region. The (3 0, -1 1) diffraction beams visible in c) are also circled in b), see text.

2. Structure calculations and adsorption energies for the hexagonal, 1 ML water network.

Calculations were performed using VASP with the optB86b-vdW exchange-correlation functional, as described in the Methods section. The Cu(511) slab consisted of 6 layers with the bottom 2 layers fixed and had an optimized lattice parameter of 3.605 Å, almost identical to the experimental value. Calculations for bulk ice using this functional yielded a lattice parameter 3% smaller than the experimental value and a binding energy of 72.4 kJ/mol, which reduces to 71.4 kJ/mol when the structure is constrained to the experimental ice lattice spacing.

Figure S3 shows the structures calculated using a (3 0, -1 1) unit cell, the smallest unit cell consistent with a hexagonal 1 ML water network. All figures shown here have the step up direction and terrace down direction from left to right, as shown in Fig. 1a. The terminology used to describe the sites is defined in the final frame of Fig. S3. Favorable structures have both the water molecules on the Cu step binding flat in a double donor arrangement, with one other double donor species (circled light blue in Fig. S3) and the remaining 3 sites single donor species, aligned either H-down towards Cu or H-up (circled yellow). The 9 best structures we found have an adsorption energy of -75.2±0.4 kJ/mol and include arrangements where all the single donor species are H-down (A, B, C, E, F) or one water above the step edge is aligned H-up (D, G, H, I). These structures all have the double donor on the terrace above the step, moving this to below the step (L, N, O) is slightly less favorable. Moving the H-up site from above the step (D, G, H, I) to below it (J, K, M, P) is marginally (≥0.7 kJ/mol) less favorable. In contrast to these small changes in overall adsorption energy, disrupting water on the Cu step by reorienting one of them from flat to H-up is extremely unfavorable (structure Q), while there is no discernable change in adsorption energy if the water on the step both donate to the upper terrace (structures E, F) or the lower terrace (all other structures). Changing the direction in which the OH points in adjacent water chains (B and C) also has no discernable effect on the adsorption energy.

Although LEED and HAS show the overall corrugation of the surface (i.e. the water or O sites) follow a long range (3 0, -1 1) repeat, the H positions are not constrained to follow such an ordered arrangement. Using a larger surface repeat allows more and different H arrangements within the overall hexagonal water network, particularly in the relative location of the H-up and double donor sites on the Cu terraces. Figure S4 shows the effect of doubling the repeat distance perpendicular to the steps using a (3 0, 1 2) unit cell to allow more complex proton arrangements. Recalculating structures A and D (Fig. S3) in the new unit cell (R and W, Fig. S4) finds the energy changes by ≤0.1 kJ/mol. In the larger unit cell, structures containing only H-down water (structures R, U, V) have identical adsorption energies to

those with either one (S, T) or two (W, X, Y) waters H-up. Placing both double donor sites in the same half of the rectangular unit cell is extremely unfavorable (Fig. S4 structure Z).

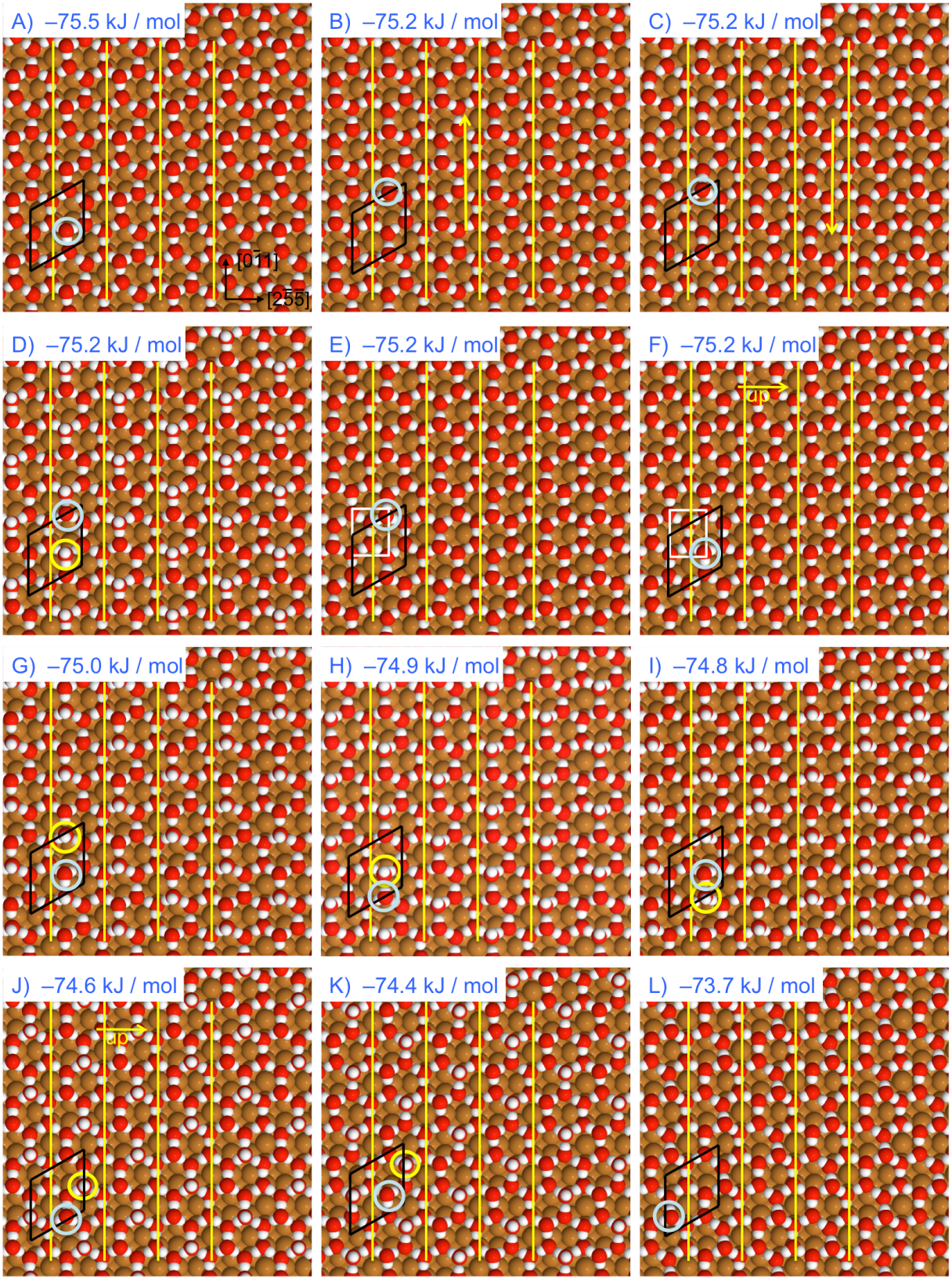

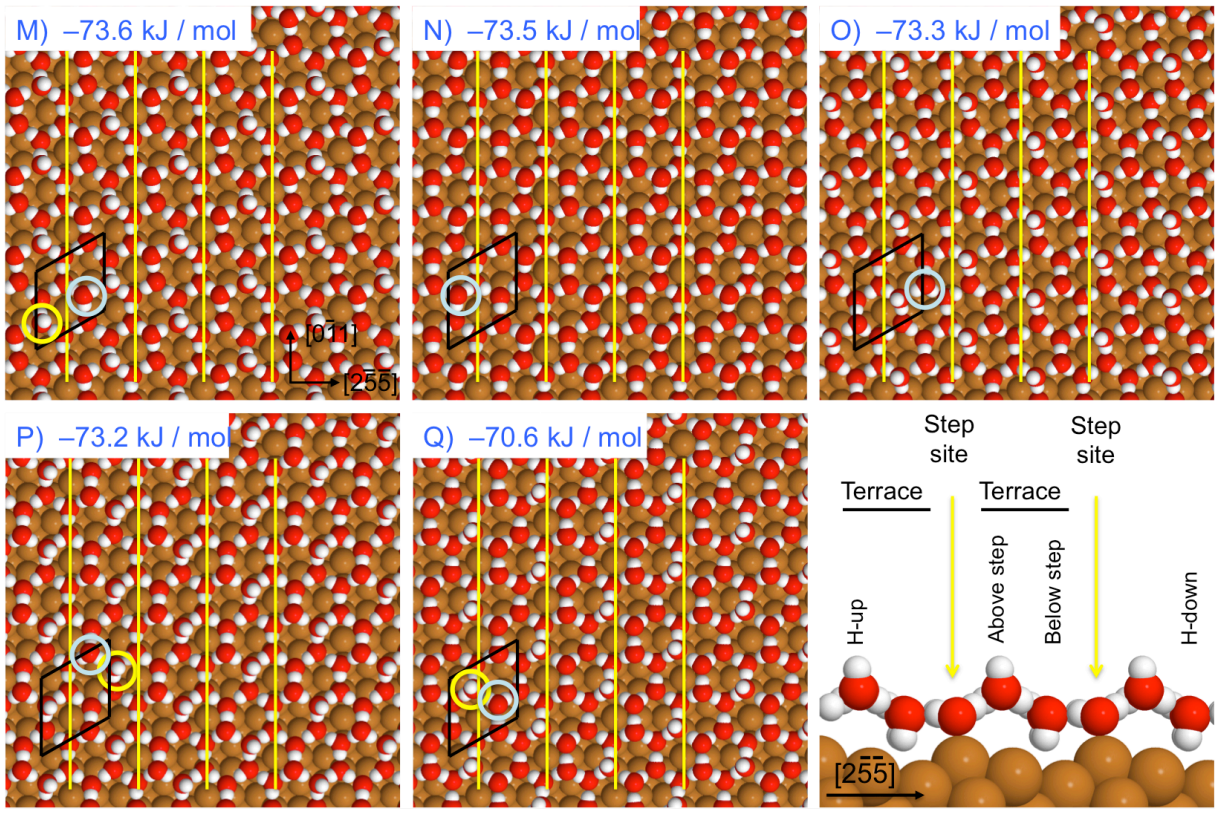

Figure S3. Calculated structures and adsorption energies for the hexagonal 1 ML water structure, calculated in the (3 0, -1 1) unit cell (shown in black). Structures are listed in order of increasing adsorption energy (decreasing binding energy) and the final frame indicates the nomenclature for the water sites used in discussion of the structures. The Cu steps are indicated by the yellow lines, water on the terrace with a double H donor geometry is circled light blue and the H-up sites in yellow. The white rectangle (E, F) shows structures where both water molecules on the step edge donate to the upper terrace, whereas all other structures have both step water molecules donating to the lower terrace. The yellow arrows in frames B and C show the reversal of the OH direction between these two structures, which causes no change in adsorption energy.

The DFT calculations indicate that the adsorption energy of water is unchanged when 1 in 6 water molecules in the first layer are aligned H-up instead of H-down. To confirm that this conclusion is not dependent on the choice of DFT functional, we repeated calculations for the best H-down and H-up structures (Fig. S3 A and D) using rev-vdW-DF2 [5] in the (3 0, -1 1) unit cell. The different functional gives almost exactly the same difference in energy ($\Delta E < 0.2$ kJ/mol) as optB86b-vdW for the two best H-down and H-up structures. Figure S5 shows STM simulations for the best H-down (A) and H-up arrangements (D). The presence of H-up water dominates the STM contrast, the other structure being

invisible, whereas water rings can be resolved for entirely H-down structures, consistent with the conclusion that water forms disordered H-up rows parallel to the Cu steps.

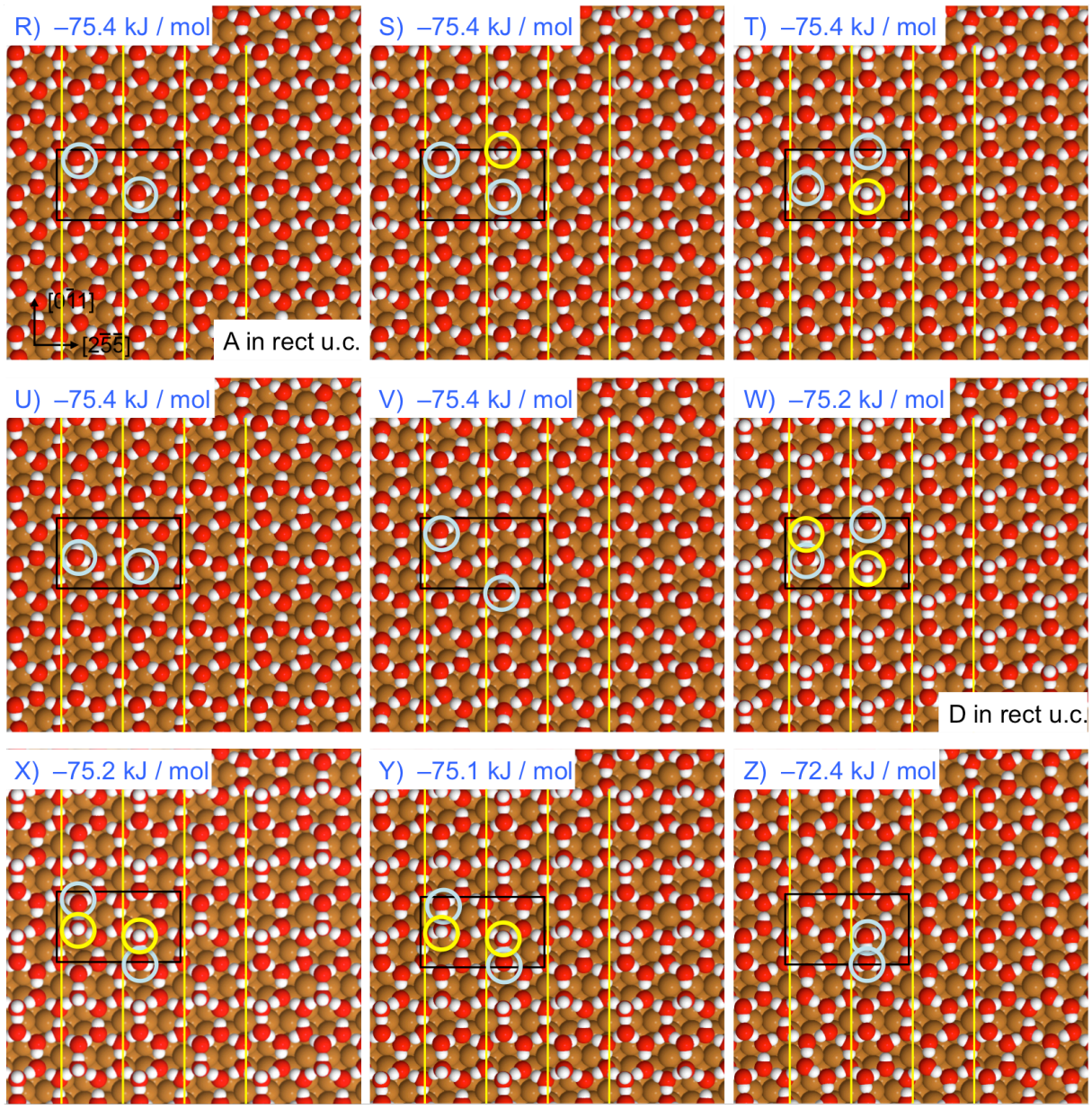

Figure S4. Adsorption energies of structures calculated using a rectangular (3 0, 1 2) unit cell, twice as big as the (3 0, -1 1) cell used in Fig S3. Water molecules that lie along the step edge are bound flat in the double donor geometry. The two water molecules on the terrace that have a double H donor geometry are circled in light blue, while any H-up sites are circled in yellow. Structures R and W have the same proton arrangement as structures A and D in Fig. S3.

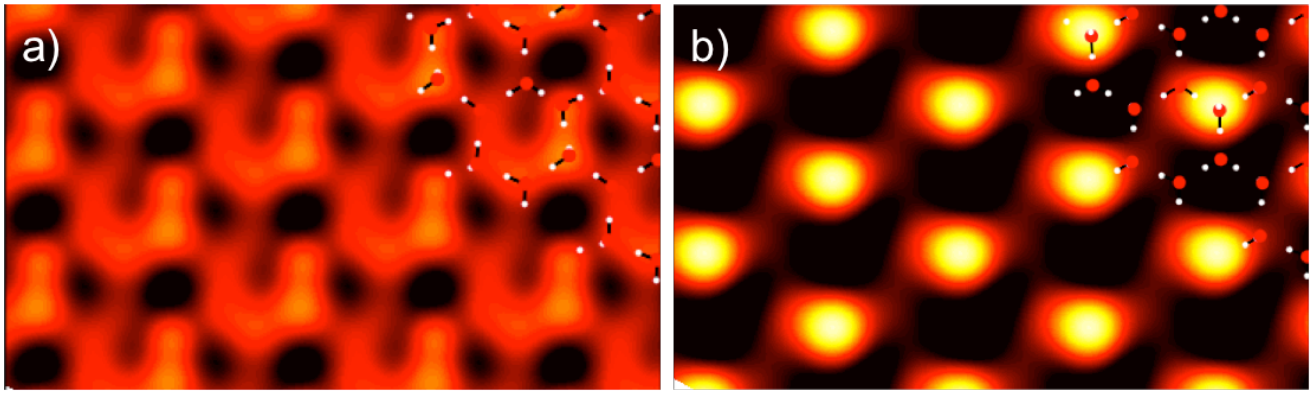

Figure S5. STM simulations of structures from DFT. a) the best H-down structure (Fig S3A) and best H-up structure (Fig S3D) in the (3 0, -1 1) unit cell. Simulations made at 0.1 eV with the same vertical contrast range. H-up water dominates the images, obscuring the water rings below.

3. Additional structures calculated for 2 and 3 layers of water.

Figure S6 shows two layer water structures calculated in the (3 0, -1 1) unit cell. Stable arrangements all have 3 H-bonds between each hexamer in the first and second layer, forming a buckled structure very similar to that of bulk ice. The two layer film has a binding energy 3.8 kJ/mol less than the first layer, implying second layer water is less stable than when bound in a monolayer. The two best structures we found have hexagonal water layers arranged on top of first layer structure K (Fig. S3) in either an AA or an AB arrangement (Fig. S6 a and b). In this arrangement the first layer has one H-up water below the step donating to the second layer, while the double donor species on the terrace (circled blue, Fig. S3K) and one water on the step act as H accepters. Accepting a proton from the second layer causes these waters to buckle away from the Cu surface, reducing the interaction with the metal but creating stronger H-bonds with a more tetrahedral water geometry. Structure S6c is derived from the best single H-up first layer structure (D, Fig. S3), the second layer binding to the first by forming tetramer rings with alternating up-down H-donation to water on the terrace above the step. This structure is less stable than arrangements that more closely resemble bulk ice. Structures S6(d,e) have two water molecules in next nearest neighbor sites on the Cu terrace aligned H-up to bind to the second layer, forming a rather more distorted ice arrangement. Figure S6f shows the 'sandwich' structure formed by aligning all the uncoordinated H atoms in the first layer H-up such that they alternate with the H-down water in the second layer. This creates an H-bond between the each water in the two layers, but at the expense of forming a flat, strained geometry, quite unlike ice. This structure is significantly (5.5 kJ/mol) less stable than the 'icelike' structures (AA and AB), whereas calculations find this arrangement is the most stable 2 layer structure for water on plane surfaces, such as Pt(111). Arrangements where all the water in the first layer point H-down were not stable in the presence of a second water layer.

Bonding a third layer of hexagonal water on top of the best two layer structures (AA and AB, Fig. S6) creates the structures shown in Fig. S7, with a binding energy 71.6 kJ/mol, very similar to that of the 2 layer film. The addition of the third layer has negligible effect on the water-Cu interface layer, the geometry of water in the top two layers being almost identical to that of bulk ice. The calculated binding energy of water in the 3 layer film (71.6 kJ/mol) is close to that calculated for bulk ice. The DFT functional used here gives a bulk ice binding energy of 72.4 kJ/mol at the optimum ice lattice parameter and 71.4 kJ/mol at the experimental spacing (4.52 Å). The close correspondence between the binding energy of the multilayer films and that of bulk 3D ice indicates there is no driving force for water to segregate into 3D ice clusters and monolayer on Cu(511) in the manner that occurs on flat surfaces.

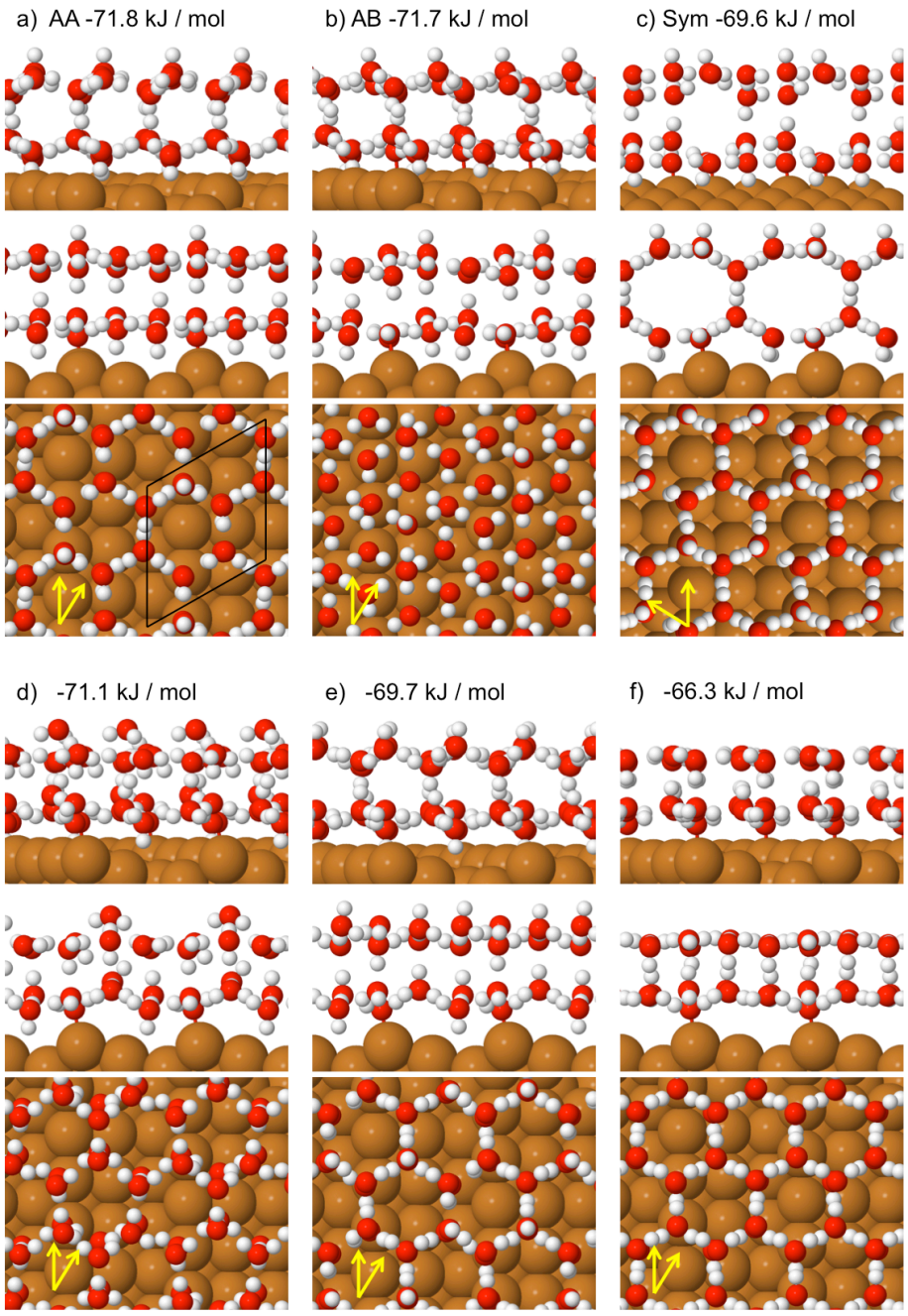

Figure S6. Calculated structures and adsorption energy for 2 layers of water on the Cu(511) surface. The unit cell is shown by the black lines in frame a) and the top two frames in each image show side views of the water structure looking along the directions marked by the arrows in each frame, the lower frame being along the $[0\bar{1}1]$ Cu step.

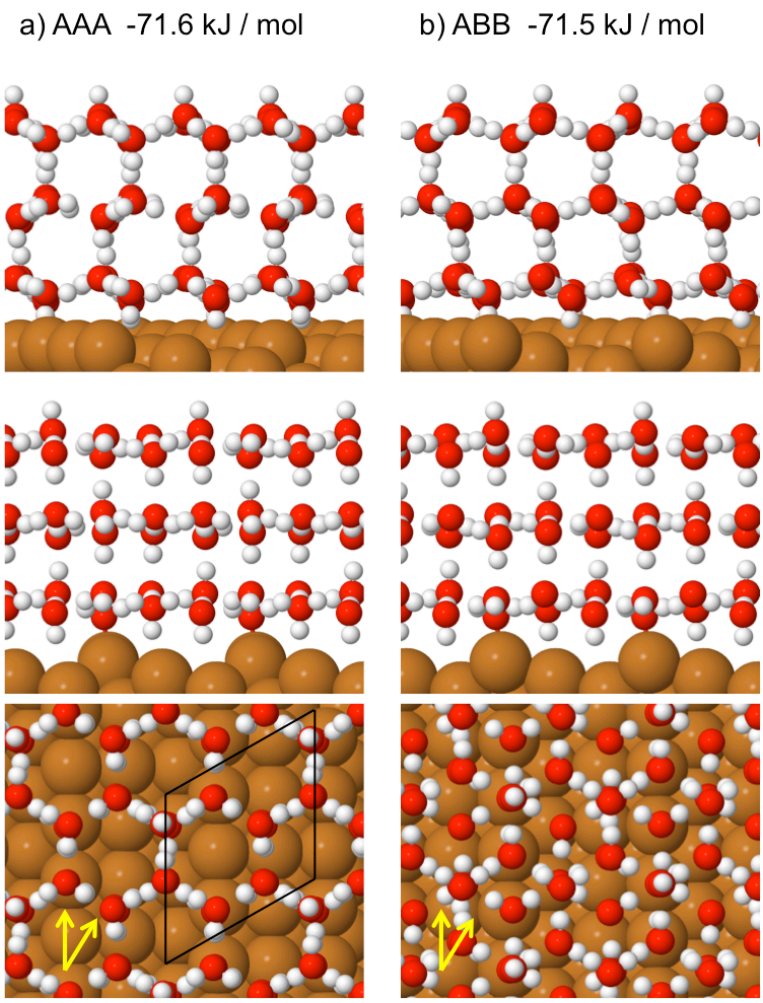

Figure S7. Calculated structures and adsorption energy for 3 layers of water on Cu(511). The unit cell is shown by the black lines in frame a), with side views of the water structure shown looking along the directions marked by the arrows in each frame, the lower frame being the $[0\bar{1}1]$ Cu step.

4. Entropic contributions to the free energy of 2D versus 3D structures.

Apart from the enthalpy contribution to the free energy of adsorption, we should also consider the role of entropic contributions and how these vary for different structures. Evidence for disorder in the local water H arrangement comes from STM images of the hexagonal structure (Fig. 2e, S2a) and implies that different water proton arrangements have similar energies, contributing Pauling entropy to stabilize the system. DFT finds ten (30,-11) structures calculated in Fig. S3 have a binding energy less than kT (0.8 kJ/mol) above the lowest energy state at 100 K (taken as the temperature at which H becomes immobile), consistent with disorder in the monolayer structure. For a completely disordered H-down water layer, the location of H between O contributes ~0.65 kJ/mol [6] stabilization to the 2D network, just 0.3 kJ/mol more than for a 3D cluster. The water layer on Cu(511) has greater constraint on the H-bond network, since the energy is influenced by the local H-bond arrangement. Assuming the (30,-11)

hexamers do not interact with each other energetically we can estimate the residual entropy using the DFT structures calculated (Fig. S3) and their symmetry equivalents, giving a contribution of 0.5 kJ/mol at 100 K, consistent with the Feibelman and Alavi estimate [6] and just 0.15 kJ/mol greater than for bulk ice. A second contribution comes from the difference in vibrational energy of the 2D film compared to the 3D ice, which we calculate in VASP using the harmonic approximation for phonons at the G point [7]. Although the zero point energy term is significant, it is almost identical between bulk ice and the 2D structures, (different 2D arrangements have a vibrational entropy term differing by ~0.02 kJ/mol), the vibrational term giving an overall contribution of -0.16 kJ/mol to stabilize bulk ice over the 2D film at 100 K. The net entropic contribution to the free energy of the 2D layer versus a 3D bulk ice structure is -0.01 kJ/mol at 100 K. The biggest source of error here is the estimation of the Pauling entropy for the different 2D structures, which is estimated as no more +/-0.2 kJ/mol from analogy to the fully proton disordered structure [6]. The entropy contribution to the difference in free energy between structures is therefore small compared to the absolute accuracy of the DFT calculations, or to the difference in binding energy between different water structures (75.5 kJ/mol for the 2D layer and 72.4 kJ/mol for bulk ice). Although small, enthalpy differences dominate the stability of the wetting phase versus bulk ice formation, consistent with previous studies that also concluded the enthalpy term dominates when comparing wetting versus bulk ice structures [6,8]. This situation may be different in systems where water dissociates at the surface, or low dimensional or gaseous phases are present.

References

1 Lin, C., Avidor, N., Corem, G., Godsi, O., Alexandrowicz, G., Darling, G. R. & Hodgson, A. Two-Dimensional Wetting of a Stepped Copper Surface. *Phys. Rev.Lett.* **120**, 076101 (2018).

2 McBride, F., Darling, G. R., Pussi, K. & Hodgson, A. Tailoring the structure of water at a metal surface: a structural analysis of the water bilayer formed on an alloy template. *Phys. Rev. Lett.* **106**, 226101 (2011).

3 McBride, F., Darling, G. R., Pussi, K., Lucas, C. A., Grunder, Y., Darlington, M., Brownrigg, A. & Hodgson, A. The Influence of Water and Hydroxyl on a Bimetallic (root 3 x root 3)R30 degrees Sn/Pt Surface Alloy. *J. Phys. Chem. C* **117**, 4032 (2013).

4 Massey, A., McBride, F., Darling, G. R., Nakamura, M. & Hodgson, A. The role of lattice parameter in water adsorption and wetting of a solid surface. *Phys. Chem. Chem. Phys.* **16**, 24018 (2014).

5 Hamada, I. van der Waals density functional made accurate. *Phys. Rev. B* **89**, 121103 (2014).

6 Feibelman, P. J. & Alavi, A. Entropy of H_2O wetting layers. *J. Phys. Chem. B* **108**, 14362 (2004).

7 Loffreda, D. Theoretical insight of adsorption thermodynamics of multifunctional molecules on metal surfaces. *Surf. Sci.* **600**, 2103 (2006).

8 Feibelman, P. J. A wetting layer breaks the ice rules. *Chem. Phys. Lett.* **410**, 120 (2005).